RED GIANT BRANCH NUCLEOSYNTHESIS AND MIXING IN THE MAGELLANIC CLOUDS

Caroline McCormick
Department of Astronomy, University of Virginia

Advisors: Dr. Steven R. Majewski and Dr. Verne V. Smith
April 18, 2024

Abstract

Stars dictate the chemical makeup of the universe as they produce almost all existing elements today. The aim of this work is to use stellar chemical abundances to test theoretical predictions of stellar evolution during the red giant branch (RGB) phase. Furthermore, we aim to study how a star's evolution changes for changing mass and metallicity (heavy-element content). From the APOGEE survey, we have identified a sample of 5,911 low-mass, RGB stars in Large and Small Magellanic Clouds—two nearby galaxies. We derived luminosities, masses, and ^{12}C/^{13}C surface abundance ratios (i.e. a tracer of RGB nucleosynthesis and mixing processes) for 754 stars. We investigated how these ^{12}C/^{13}C ratios change as a function of mass and metallicity. Our results suggest that an additional mixing episode not explained by standard stellar evolution theory is necessary to justify the low ^{12}C/^{13}C abundances. We also find that mixing on the RGB is not as prominent for higher mass stars (i.e. ^{12}C/^{13}C is higher for higher mass stars) as predicted by the additional mixing model. Future efforts will be aimed at deriving more ^{12}C/^{13}C, tracking how [C/N] (another evolution tracer) changes with stellar parameters, and investigating more closely how these ratios change with metallicity.

Introduction

Understanding how stars evolve is one of the most critical puzzle pieces necessary for explaining the chemical evolution of galaxies and the universe as a whole. Besides the Big Bang, stars are the primary producer of nearly all chemical elements that we see in the universe today. Throughout their lifetime, stars undergo many episodes of a process called nucleosynthesis (i.e., the creation of nucleii), which fuses less massive elements into progressively heavier elements. This process occurs deep within stellar interiors, and the mixing of internal layers often brings newly made heavy elements to the surface of the star. This material is then eventually returned to the interstellar medium (ISM) either through mass loss at the surface or when the star dies.

Relatively speaking, the theory of stellar evolution is fairly well understood. However, there still exists uncertainties in late evolution nucleosynthesis and mixing processes, particularly in a phase of evolution known as the red giant branch (RGB). During the RGB, low-mass stars[1] undergo H fusion into He (often referred to as "H burning") in a thin shell surrounding the core of the star. Meanwhile, the envelope of the star extends outward becoming large, cool, and convective.

A major mixing episode known as the first dredge up (FDU) occurs at the beginning of

[1] Low-mass stars here are defined as stars in the approximate mass range 0.8-2.5$M_{\odot}$, though this range can change depending on the proportion of heavy elements in the star.

the RGB phase. During the FDU, the convective envelope extends into the layers where nucleosynthesis had occurred earlier in the star's life, bringing processed material to the surface of the star. Most notably, ^{13}C and ^{14}N are dredged up to the surface of the star during this event due to the fact that H burning in part occurs by a process called the carbon-nitrogen-oxygen (CNO) cycle, which creates and uses C, N, O, and their isotopes as catalysts to fuse H into He (e.g., Palacios et al. 2003; Charbonnel & Lagarde 2010).

Standard stellar evolution theory has predicted that the FDU is the only major mixing episode to occur during this phase of evolution. However, observations of RGB stars (e.g., Gilroy 1989; Tautvaišienė et al. 2013; Takeda et al. 2019; McCormick et al. 2023 and references therein) have shown that the surface abundances of C, N, and their isotopes are altered further than the FDU predicts in low-mass stars on the RGB. Therefore, an additional mixing event is thought to occur in the late stages of the RGB phase. The exact physical process(es) that cause this extra mixing is still unknown, though many possibilities have been suggested (see, e.g., Boothroyd et al. 1995; Charbonnel 1995; Busso et al. 2007; Palacios et al. 2006 and references therein). A popular idea is that the extra mixing is due, at least in part, to an instability naturally occurring within stellar interiors on the RGB known as the thermohaline instability (e.g., Charbonnel & Zahn 2007). This instability induces mixing just outside the H-burning shell, and models have shown that it can connect to the convective envelope (e.g., Lagarde et al. 2012), which funnels more nucleosynthesis byproducts (e.g., ^{13}C, ^{14}N) to the surface of the star. The ^{12}C/^{13}C abundance ratio is typically used to probe this RGB nucleosynthesis and mixing, as it has been shown to change dramatically[2] on the RGB due to mixing episodes (see above references to observations).

[2]Often, ^{12}C/^{13}C starts around 90 before the FDU and drops to approximately 10-20 near the tip of the RGB.

To date, the majority of observational evidence for RGB nucleosynthesis and mixing processes are for stars in our own Milky Way galaxy that have properties similar to our Sun. Specifically, most of the stars observed have a similar overall proportion of heavy elements (i.e., "metallicity"; often denoted by "[Fe/H]"). Changing the metallicity of a star alters that star's evolution since the amount and type of material it possesses dictates how long it can undergo nuclear fusion. Similarly, more massive stars burn through their material quicker to provide enough pressure support from gravity to be stable, which leads to shorter episodes of nucleosynthesis and mixing and shorter lifetimes.

In this work, we seek to add to the body of observational evidence for RGB nucleosynthesis and mixing processes by providing a large sample of surface ^{12}C/^{13}C abundances to trace internal stellar evolutionary processes. We aim to test theoretical predictions of these abundances to better understand how these processes are affected by a range of stellar properties such as mass and metallicity to gain a more global understanding of how stars evolve.

We do so by studying large samples of stars in two low-metallicity, satellite galaxies of the Milky Way known as the Large Magellanic Cloud (LMC) and the Small Magellanic Cloud (SMC). In this paper, we first describe the data we use to accomplish these goals. It is then explained how we estimated stellar properties such as luminosity and mass, along with how we derived chemical abundances using stellar spectra. Finally, we show our current results and conclude by interpreting these results and describing our next steps.

Data

The data used in this project are from the 17th Data Release (DR17; Abdurro'uf et al. 2022) of the Sloan Digital Sky Survey IV's (SDSS-IV; Blanton et al. 2017) Apache Point Observatory Galactic Evolution Experiment (APOGEE; Majewski et al. 2017),

which combines data from the APOGEE and APOGEE-2 surveys. The Magellanic Clouds (MCs) were observed using the APOGEE-S spectrograph Wilson et al. (2019) on the 2.5-meter du Pont Telescope (Bowen & Vaughan, 1973) at Las Campanas Observatory in Chile. Targeting for the APOGEE survey is described in Zasowski et al. (2013), while that for the APOGEE-2 survey is described in Zasowski et al. (2017), Beaton et al. (2021), and Santana et al. (2021). The data reduction pipeline for APOGEE is described in Nidever et al. (2015).

The APOGEE survey reports near-infrared photometry from the Two Micron All Sky Survey (2MASS; Skrutskie et al. 2006) in the J, H, and K_s magnitude bands. Furthermore, APOGEE also provides stellar parameters and abundances which were derived using the APOGEE Stellar Atmospheric Parameters and Chemical Abundances Pipeline (ASPCAP; García Pérez et al. 2016) based on the FERRE code written by Allende Prieto et al. (2006). For each star, ASPCAP matches stellar atmospheric parameters to a grid of MARCS stellar atmospheres (Gustafsson et al., 2008; Jönsson et al., 2020) and derives chemical abundances using synthetic spectra and an H-band line list from Smith et al. (2021).

The MC sample in APOGEE is vast ($\backsim$13,000 stars in the LMC and $\backsim$3,000 in the SMC), so utilizing this data set will provide an unprecedented sample of stellar abundances critical for understanding stellar evolution on a large scale. Furthermore, the MCs are ideal for this type of study because the MCs have been historically well studied, and we now have highly accurate distances to the clouds, which allows for reliable estimates of stellar luminosities.

Red Giant Branch Sample Selection

To select our sample of stars from the greater APOGEE catalog, we first had to choose which stars belong to the MCs. We followed the methodology of Hasselquist et al. (2021) which implements a series of cuts based on spatial and kinematic data to select the stars likely to belong to the MCs. The specific criteria we used to choose the LMC and SMC sample can be seen in Table 1. In summary, we first chose all stars within a projected spherical distance (D) from the center of each cloud based on each star's right ascension (α) and declination (δ) coordinates. Next, we attempted to exclude any foreground Milky Way contaminates by removing any stars that have radial velocities (RV) and/or proper motions (in right ascension, μ_α, or in declination, μ_δ) differing by $\pm 3\sigma$ from the median of these quantities for the MCs.

Table 1: The spatial and kinematic parameters used to identify stars belonging to the LMC and SMC.

Quantity	LMC	SMC
α°_{center}	80.894	13.187
δ°_{center}	-69.756	-72.829
D°	12	8
RV (km/s)	(161, 370)	(66, 235)
μ_α (km/s)	(1.01, 2.62)	(0.05, 1.51)
μ_δ (km/s)	(-1.15, 1.70)	(-1.57, -0.94)

The aforementioned cuts result in stars in various phases of evolution in the MCs, so we next sought to isolate stars belonging to the RGB only. To do so, we first selected stars less luminous than the tip of the RGB (TRGB; i.e., the maximum brightness of RGB stars) based on the definition from Hoyt et al. (2018). This definition characterizes the TRGB based on 2MASS photometry and the distance modulus to each cloud (μ):

$$H < \mu - 5.94 - (1.62 \times ((J - K_s) - 1.0)) - 0.1 \quad (1)$$

Throughout this work, we use a distance modulus of 18.477 $\pm$ 0.004 mag for the LMC (Pietrzyński et al. 2019) and 18.977 $\pm$ 0.016 mag for the SMC (Graczyk et al. 2020).

To remove obvious higher mass ($> \backsim 3 M_\odot$) star contaminates, we removed stars with effective temperature (T_{eff}) greater than 5000 K. Also, near the TRGB we removed any star with H < 12.8 mag and metallicity greater than -0.55 dex since more massive

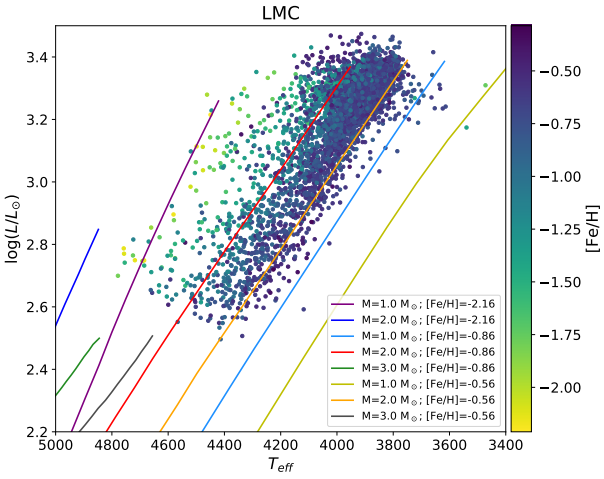

Figure 1: The HR diagram of the LMC stars in our sample colored by metallicity. Overlaid are stellar evolutionary tracks from Lagarde et al. (2012) for various masses and metallicities.

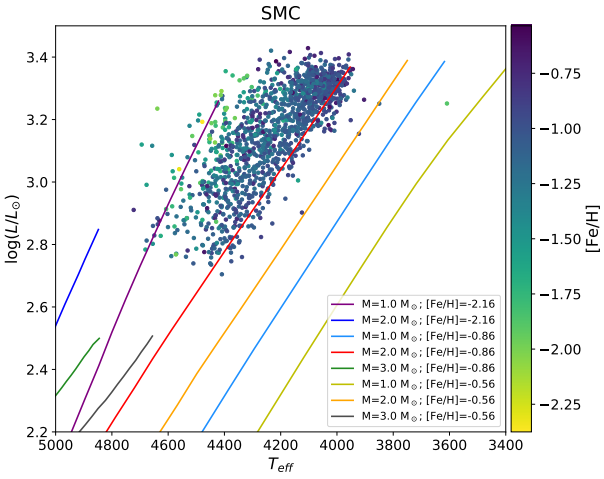

Figure 2: The same as Figure 1 but for the SMC stars.

stars typically have higher metallicities than RGB stars. Moreover, we removed stars with $(J - K_s) > 1.3$ to avoid C-rich asymptotic giant branch stars.

Finally, we required that all stars in our sample have reliable data by not having the "STAR BAD" flag set in the APOGEE catalog, which indicates that there is something untrustworthy about the data for a given star. Our data cuts resulted in 4,436 RGB stars in the LMC and 1,475 RGB stars in the SMC. Figures 1 and 2 show our sample stars in the Hertzsprung-Russell (HR) diagram.

Extinction Corrections

Observing the true brightness of stars is nearly impossible due to the fact that dust and gas in the ISM often lie along an observer's line of sight to an object. For this reason, the magnitudes we observe are extincted (i.e., the light we see appears redder in color than it is intrinsically) by varying amounts depending on the wavelength of light and the amount of material between the observer and the object.

To correct for this phenomenon, we applied extinction corrections to the photometric magnitudes in our data set. Fortunately, the APOGEE catalog provides K_s-band extinction corrections for each star in our sample. We then used the extinction law of Cardelli et al. (1989) to relate the K_s correction terms (A_{K_s}) to other photometric band correction terms (A_J and A_H):

$$\frac{A_J}{A_{Ks}} = 2.45 \quad \text{and} \quad \frac{A_H}{A_{Ks}} = 1.56 \qquad (2)$$

The extinction corrections in these infrared magnitudes are relatively small, however, it is important to incorporate them to derive as accurate as possible stellar luminosities, which are based on observed magnitudes.

Derived Quantities

Stellar Luminosity

To better understand the fundamental properties of the stars in our sample, we calculated the luminosity, or intrinsic brightness, of each star. Knowing the luminosity of a star also makes it easier to compare our data with theoretical models which often report stellar brightness as luminosity.

The stellar luminosity, in units of solar luminosities ($L_\odot$), can be calculated using the following equation:

$$L = 10^{(M_{bol,\odot} - K_{s,0} - BC_{K_s} + \mu)/2.5} L_\odot \qquad (3)$$

Here, $M_{bol,\odot}$ is the bolometric absolute magnitude of the Sun (4.74 $M_\odot$; Mamajek et al.

Table 2: The central wavelength for each chemical feature used in our spectral fitting analysis with BACCHUS to derive abundances.

Species	Wavelengths (Å)
Si	15361.2, 15376.8, 15557.8, 15884.5, 15960.1, 16060.0, 16094.8, 16129.0, 16163.7, 16170.2, 16215.7, 16241.8, 16680.8, 16828.2
C	15578.0, 15775.5, 15978.7, 16004.9, 16021.7, 16185.5, 16397.2, 16614.0, 16836.0, 16890.4
O	15373.5, 15391.0, 15569.0, 15719.7, 16052.9, 16055.5, 16650.0, 16704.8, 16714.5, 16872.0, 16909.4
N	15210.2, 15222.0, 15228.8, 15242.5, 15251.8, 15309.0, 15317.6, 15363.5, 15410.5, 15447.0, 15462.4, 15466.2, 15495.0, 15514.0, 15581.0, 15636.5, 15659.0, 15706.9, 15708.5
Mg	15231.8, 15366.9, 15693.6, 15740.7, 15749.0, 15765.7, 15879.6, 15954.5, 16365.0, 16624.7, 16632.0
^{12}C/^{13}C	15641.7, 16121.4, 16323.4, 16326.0, 16327.3, 16530.0, 16741.2, 16744.7

2015); $K_{s,0}$ is the extinction-corrected apparent K_s magnitude; BC_{K_s} is the K_s bolometric correction term from the MESA Isochrone and Stellar Track (Dotter 2016; Choi et al. 2016; Paxton et al. 2011, 2013, 2015, 2018) bolometric correction tables; and μ is the representative distance modulus to each cloud.

It is important to note that while these distance modulii are precisely known, they are the distance modulii calculated to the central regions of each cloud. Therefore, they do not account for the width of each cloud, which do start to become a significant fraction of the distance the further from the center of the cloud a star is. For this reason, we expect that stars located farther from the center of the cloud will have higher uncertainties in luminosity and mass (see next section).

Stellar Mass

Another property of stars that is necessary to know for understanding stellar evolution is mass. Unfortunately, we cannot directly measure the mass of a star, so we have to rely on indirect methods of estimating stellar mass.

One way of doing so is to use equations of stellar astrophysics that relate measurable stellar properties to mass. APOGEE derives two such properties, the stellar surface gravity ($\log g$) and effective temperature (T_{eff}), from stellar spectra by comparing the observed spectrum of each star to model spectra. Furthermore, since we now know the luminosities of our stars, the following equations can be rearranged and combined to estimate stellar masses (M):

$$L = 4\pi\sigma_{SB}R^2T_{eff}^4 \tag{4}$$

$$\log g = \log\left(\frac{GM}{R^2}\right) \tag{5}$$

$$M = \frac{10^{\log g}L}{4\pi\sigma_{SB}GT_{eff}^4} \tag{6}$$

Here, σ_{SB} is the Stefan-Boltzmann constant; G is the gravitational constant; and R is the stellar radius.

Abundances with BACCHUS

Finally, the last quantity needed for this study is the ^{12}C/^{13}C abundances. While APOGEE provides abundances for a range of chemical species, it does not report ^{12}C/^{13}C. In this work, we utilize ^{12}C/^{13}C abundances from the BACCHUS Analysis of Weak-Lines in APOGEE Spectra (BAWLAS) catalog (Hayes et al. 2022) when available for our sample stars. If these abundance ratios are not available for a sample star, we derive our own ^{12}C/^{13}C using the Brussels Automatic Code for Characterizing High accUracy

Spectra (BACCHUS; Masseron et al. 2016) software.

The BAWLAS catalog uses APOGEE DR17 spectra and the BACCHUS code to derive accurate $^{12}C/^{13}C$ ratios. However, due to a spectrum signal-to-noise restriction implemented in Hayes et al. (2022) that was relevant to that particular study, only 374 stars (373 in the LMC and 1 in the SMC) in our sample have $^{12}C/^{13}C$ abundance ratios reported in BAWLAS. Therefore, we utilized BACCHUS and performed a similar spectral analysis as done in BAWLAS to increase the number of stars with $^{12}C/^{13}C$ abundances in our sample.

We follow the methodology of Hayes et al. (2022) for our BACCHUS analysis (see Hayes et al. 2022 and Masseron et al. 2016 for a more in-depth description of how BACCHUS works). In summary, we provide APOGEE effective temperature, surface gravity, metallicity, and microturbulent velocity for each star. With these parameters, BACCHUS determines the convolution parameter for the spectrum, which describes the broadening of spectral features due to macroturbulent velocity, stellar rotation, and instrument resolution. The convolution parameter is found by deriving the abundance of the Si I lines until the abundance found by two separate methods in BACCHUS (the intensity method and the equivalent width method) match. Next, we determine abundances for C, O, N, and Mg to help with proper continuum placement and provide a baseline for features blended with these species; we iterate these abundances until they are consistent. Finally, we find the $^{12}C/^{13}C$ abundance.

BACCHUS provides abundance estimates for each chemical species and for each spectral feature that we measure for each species (see Table 2 for a list of all features attempted in our analysis). The overall $^{12}C/^{13}C$ for a given star is calculated by choosing the best-fit features (here we used the features at 16121.4 $\AA$ and 16530.0 $\AA$) and computing the average abundance using the "chi2" method abundance from BACCHUS.[3] We note that for the results presented in this paper, we only use features that are the generally well-fit for most stars (16121.4 $\AA$ and 16530.0 $\AA$). As we continue to work on this project, we aim to increase the number of features used in calculating $^{12}C/^{13}C$ for each star so that the overall ratio is not biased to those two features. So far, we have been able to add $^{12}C/^{13}C$ measurements for 380 stars (147 in the LMC and 233 in the SMC) in our sample.

Results

We present the current results for this work in Figures 3-6. Beginning with Figures 3 and 4, we show $^{12}C/^{13}C$ as a function of stellar mass colored by metallicity for the entire LMC and SMC samples, respectively. To the left on each figure are typical error bars for mass and for different ranges of $^{12}C/^{13}C$. Overlaying the data in each figure are sets of models from Lagarde et al. (2012) which convey theoretical predictions of $^{12}C/^{13}C$ for the range of stellar masses shown. Two varieties of models are shown in these figures. The first variety (solid lines) represent the standard theory of stellar evolution where the only major mixing event to occur on the RGB is the FDU. The second variety of models (dashed lines) display the predicted $^{12}C/^{13}C$ for stars that have undergone the FDU, thermohaline extra mixing, and have non-zero stellar rotation on the RGB. Furthermore, each variety of model is shown for three metallicities typical of the MCs: [Fe/H]=-2.16 (orange), [Fe/H]=-0.86 (blue), and [Fe/H]=-0.56 (gray).

From these figures, we notice that the majority of our sample stars with $^{12}C/^{13}C$ have values that fall well below the standard model predictions. We also observe a slight increase in $^{12}C/^{13}C$ for increasing stellar mass in the range 1-2$M_{\odot}$, most clearly seen in the LMC, similar to the extra mixing (dashed-

[3]The chi2 method in BACCHUS finds the abundance of each feature by squaring the differences between the synthetic and observed spectra and minimizing them.

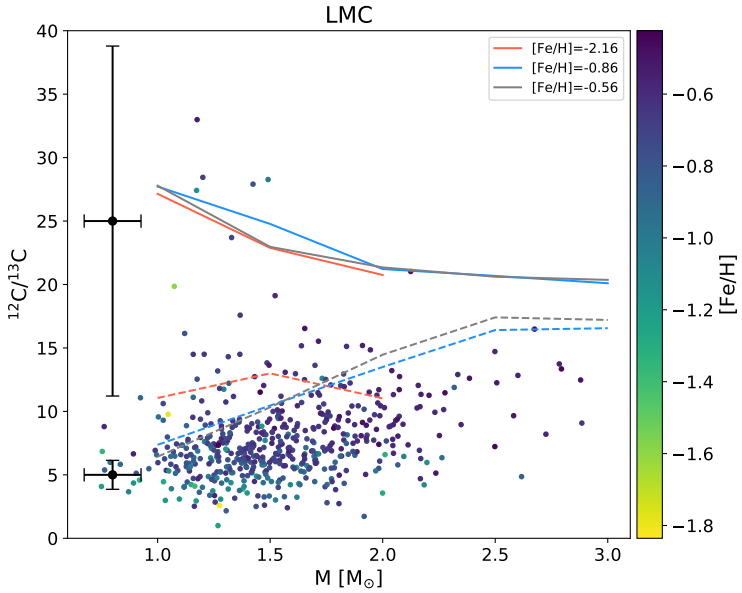

Figure 3: The $^{12}C/^{13}C$ ratio as a function of stellar mass colored by metallicity for the LMC stars. Typical uncertainties in $^{12}C/^{13}C$ and mass are shown on the left. Overlaid are models from Lagarde et al. (2012) varying in metallicity. Solid-line models show the $^{12}C/^{13}C$ predictions for standard RGB evolution (i.e., only FDU mixing on the RGB), whereas dashed-line models show $^{12}C/^{13}C$ predictions for RGB evolution including FDU, thermohaline extra mixing, and stellar rotation.

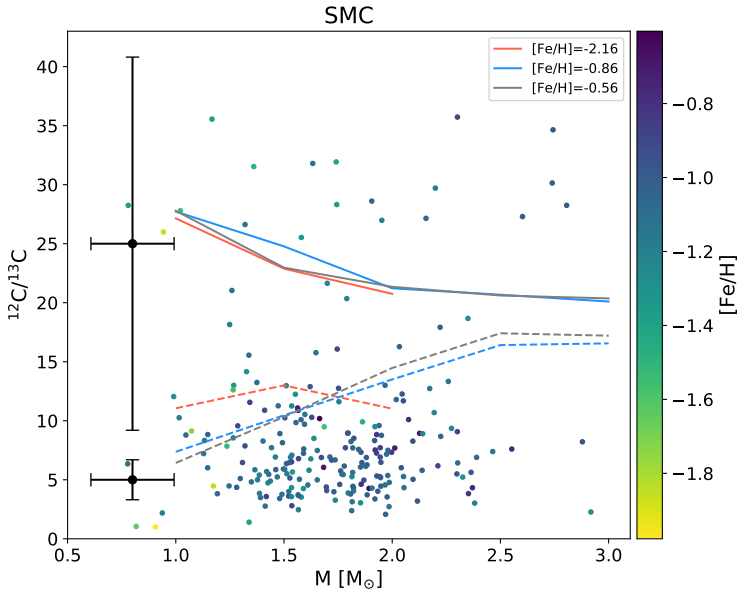

Figure 4: The same as Figure 3 but for the SMC.

line) model predictions. The trend in metallicity, however, is not as clearly seen in these figures.

To better observe how $^{12}C/^{13}C$ changes with mass excluding the effects of metallicity, we display the $^{12}C/^{13}C$ as a function of mass for small ranges of metallicity, essentially approximating metallicity as constant, in Figures 5 and 6 for the LMC and SMC, respectively. Here, the same models overlay the data, and this time we color the points by luminosity.

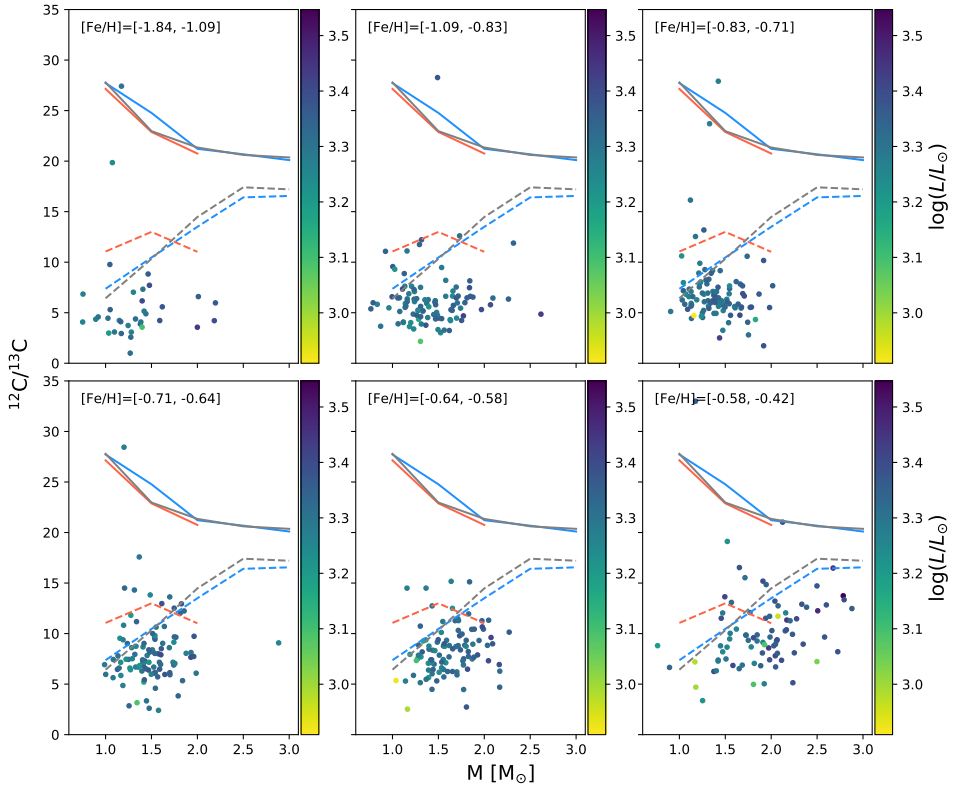

Figure 5: The $^{12}C/^{13}C$ ratio as a function of stellar mass in small ranges of metallicity colored by luminosity for the LMC stars. Overlaid are the models described in Figure 3.

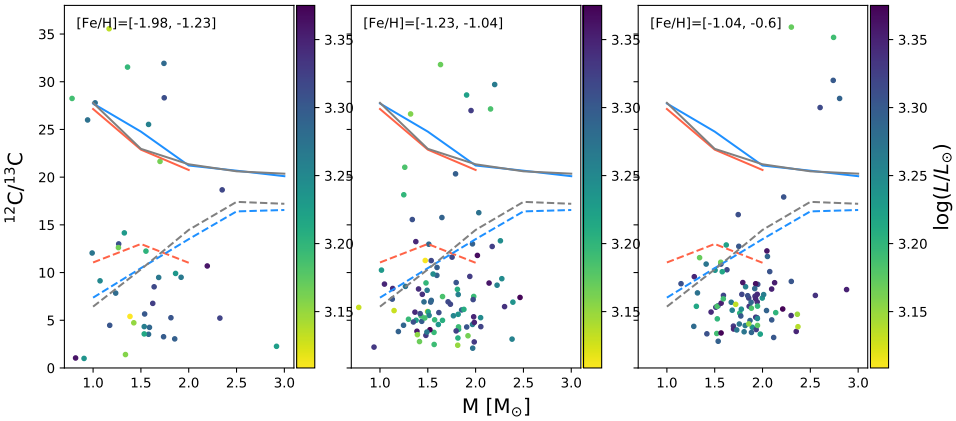

Figure 6: The same as Figure 5 but for the SMC.

We recover the same trend of decreasing $^{12}C/^{13}C$ with decreasing mass for the three highest metallicity bins in the LMC and for all three metallicity bins in the SMC. It is not as clear if the $^{12}C/^{13}C$-mass trend exists in the lower metallicity LMC bins, perhaps due to an insufficient amount of data in those bins.

It is also important to note that so far, we have only derived $^{12}C/^{13}C$ abundances for stars near the TRGB, so these figures are far from complete in characterizing the full extent of RGB $^{12}C/^{13}C$ abundance changes.

Conclusions

From our current results, we can conclude that the observed $^{12}C/^{13}C$ are in disagreement with the standard stellar evolution predictions of $^{12}C/^{13}C$ surface abundances in RGB

stars, meaning that there is an important piece of physics missing from our idea of stellar evolution based on the standard model prescription. In fact, the $^{12}C/^{13}C$ ratios most closely align with the model predicting that extra mixing occurs on the RGB, suggesting that this process is necessary to explain the $^{12}C/^{13}C$ abundances.

Furthermore, we find that in almost all of our bins of nearly constant metallicity (with the lowest-metallicity LMC bins being inconclusive), the $^{12}C/^{13}C$ reproduces the expected trend that lower mass stars tend to have lower $^{12}C/^{13}C$ values than higher mass stars at roughly the same evolutionary phase (i.e. the TRGB). Therefore, the idea that lower mass stars experience either more extra mixing or more efficient extra mixing appears to be supported by the data.

In summary, we have derived stellar luminosities, masses, and $^{12}C/^{13}C$ surface abundances so far for 380 stars adding to the BAWLAS catalog overlap of our sample which provided 374 stars with measured $^{12}C/^{13}C$. We investigated RGB nucleosynthesis and mixing processes by comparing how the $^{12}C/^{13}C$ changes with mass and metallicity against model predictions incorporating different RGB mixing processes. We found that the data agrees more closely with the model including an extra mixing mechanism, implying that some form of extra mixing is necessary to explain observations. Furthermore, we recover expected $^{12}C/^{13}C$ trends in mass, but it is not immediately clear if there is one in metallicity. Future effort will be focused on isolating the effect of metallicity on $^{12}C/^{13}C$. We also aim to incorporate more $^{12}C/^{13}C$ abundances from our 4,436-star LMC sample and 1,475-star SMC sample spanning even greater ranges of stellar parameters, especially less luminous stars to cover more of the RGB. We also aim to derive reliable [C/N] ratios and see how it changes with stellar parameters since ^{14}N is also expected to be dredged up by mixing.

Acknowledgements

CM would like to acknowledge the collaborators on this project and thank them for their support: Steven Majewski, Verne Smith, Christian Hayes, Katia Cunha, and Thomas Masseron.

Funding for the Sloan Digital Sky Survey IV has been provided by the Alfred P. Sloan Foundation, the U.S. Department of Energy Office of Science, and the Participating Institutions.

SDSS-IV acknowledges support and resources from the Center for High Performance Computing at the University of Utah. The SDSS website is www.sdss4.org.

SDSS-IV is managed by the Astrophysical Research Consortium for the Participating Institutions of the SDSS Collaboration including the Brazilian Participation Group, the Carnegie Institution for Science, Carnegie Mellon University, Center for Astrophysics — Harvard & Smithsonian, the Chilean Participation Group, the French Participation Group, Instituto de Astrofísica de Canarias, The Johns Hopkins University, Kavli Institute for the Physics and Mathematics of the Universe (IPMU) / University of Tokyo, the Korean Participation Group, Lawrence Berkeley National Laboratory, Leibniz Institut für Astrophysik Potsdam (AIP), Max-Planck-Institut für Astronomie (MPIA Heidelberg), Max-Planck-Institut für Astrophysik (MPA Garching), Max-Planck-Institut für Extraterrestrische Physik (MPE), National Astronomical Observatories of China, New Mexico State University, New York University, University of Notre Dame, Observatário Nacional / MCTI, The Ohio State University, Pennsylvania State University, Shanghai Astronomical Observatory, United Kingdom Participation Group, Universidad Nacional Autónoma de México, University of Arizona, University of Colorado Boulder, University of Oxford, University of Portsmouth, University of Utah, University of Virginia, University of Washington, University of Wisconsin, Vanderbilt University, and Yale University.

References

Abdurro'uf et al., 2022, ApJS, 259, 35

Allende Prieto C., Beers T. C., Wilhelm R., Newberg H. J., Rockosi C. M., Yanny B., Lee Y. S., 2006, ApJ, 636, 804

Beaton R. L., et al., 2021, AJ, 162, 302

Blanton M. R., et al., 2017, AJ, 154, 28

Boothroyd A. I., Sackmann I. J., Wasserburg G. J., 1995, , 442, L21

Bowen I. S., Vaughan A. H. J., 1973, Appl. Opt., 12, 1430

Busso M., Wasserburg G. J., Nollett K. M., Calandra A., 2007, ApJ, 671, 802

Cardelli J. A., Clayton G. C., Mathis J. S., 1989, ApJ, 345, 245

Charbonnel C., 1995, , 453, L41

Charbonnel C., Lagarde N., 2010, A&A, 522, A10

Charbonnel C., Zahn J. P., 2007, A&A, 467, L15

Choi J., Dotter A., Conroy C., Cantiello M., Paxton B., Johnson B. D., 2016, ApJ, 823, 102

Dotter A., 2016, ApJS, 222, 8

García Pérez A. E., et al., 2016, AJ, 151, 144

Gilroy K. K., 1989, ApJ, 347, 835

Graczyk D., et al., 2020, ApJ, 904, 13

Gustafsson B., Edvardsson B., Eriksson K., Jørgensen U. G., Nordlund Å., Plez B., 2008, A&A, 486, 951

Hasselquist S., et al., 2021, ApJ, 923, 172

Hayes C. R., et al., 2022, ApJS, 262, 34

Hoyt T. J., et al., 2018, ApJ, 858, 12

Jönsson H., et al., 2020, AJ, 160, 120

Lagarde N., Decressin T., Charbonnel C., Eggenberger P., Ekström S., Palacios A., 2012, A&A, 543, A108

Majewski S. R., et al., 2017, AJ, 154, 94

Mamajek E. E., et al., 2015, arXiv e-prints, p. arXiv:1510.06262

Masseron T., Merle T., Hawkins K., 2016, BACCHUS: Brussels Automatic Code for Characterizing High accUracy Spectra, Astrophysics Source Code Library, record ascl:1605.004 (ascl:1605.004)

McCormick C., et al., 2023, MNRAS, 524, 4418

Nidever D. L., et al., 2015, AJ, 150, 173

Palacios A., Talon S., Charbonnel C., Forestini M., 2003, A&A, 399, 603

Palacios A., Charbonnel C., Talon S., Siess L., 2006, A&A, 453, 261

Paxton B., Bildsten L., Dotter A., Herwig F., Lesaffre P., Timmes F., 2011, ApJS, 192, 3

Paxton B., et al., 2013, ApJS, 208, 4

Paxton B., et al., 2015, ApJS, 220, 15

Paxton B., et al., 2018, ApJS, 234, 34

Pietrzyński G., et al., 2019, Nature, 567, 200

Santana F. A., et al., 2021, AJ, 162, 303

Skrutskie M. F., et al., 2006, AJ, 131, 1163

Smith V. V., et al., 2021, AJ, 161, 254

Takeda Y., Omiya M., Harakawa H., Sato B., 2019, PASJ, 71, 119

Tautvaišienė G., Barisevičius G., Chorniy Y., Ilyin I., Puzeras E., 2013, MNRAS, 430, 621

Wilson J. C., et al., 2019, PASP, 131, 055001

Zasowski G., et al., 2013, AJ, 146, 81

Zasowski G., et al., 2017, AJ, 154, 198